Title
Terahertz quantum cascade VECSEL with watt-level output power

Journal
Applied Physics Letters, 113(1)

ISSN
0003-6951

Authors
Curwen, Christopher A
Reno, John L
Williams, Benjamin S

Publication Date
2018-07-02

DOI
10.1063/1.5033910

Peer reviewed

Terahertz Quantum Cascade VECSEL with Watt-Level Output Power

Christopher A. Curwen,[1,a)] John L. Reno,[2] and Benjamin S. Williams[1]

[1]*Department of Electrical and Computer Engineering, University of California, Los Angeles, California 90095, USA*

[2]*Sandia National Laboratories, Center of Integrated Nanotechnologies, MS 1303, Albuquerque, New Mexico 87185, USA*

We report a terahertz quantum-cascade vertical-external-cavity surface-emitting laser (QC-VECSEL) whose output power is scaled up to watt-level by using an amplifying metasurface designed for increased power density. The metasurface is composed of a subwavelength array of metal-metal waveguide antenna-coupled sub-cavities loaded with terahertz quantum-cascade gain material. Unlike previously demonstrated THz QC-VECSELs, the sub-cavities operate on their third-order lateral modal resonance (TM_{03}), instead of their first-order (TM_{01}) resonance. This results in a metasurface with a higher spatial density of gain material, leading to increased output power per metasurface area. In pulsed mode operation, peak THz output powers up to 830 mW at 77 K, and 1.35 W at 6 K are observed, while a single-mode spectrum and a low divergence beam pattern is maintained. In addition, piezoelectric control of the cavity length allows approximately 50 GHz of continuous, single-mode tuning without significant effect on output power or beam quality.

THE MANUSCRIPT

Terahertz quantum-cascade (QC) lasers have emerged as a promising source of high-power, coherent terahertz radiation.[1] There are two existing methods for waveguiding in THz QC-lasers. The first is the surface plasmon (SP) waveguide[2], in which the multiple-quantum-well gain material is grown above a highly doped semiconductor layer on a semi-insulating substrate which supports a loosely confined surface-plasmon mode. The second is the metal-metal waveguide[3], in which the gain material is sandwiched between two metal layers to create a set of highly confined modes with sub-wavelength transverse dimensions. Multi-watt power levels have been demonstrated from SP waveguides, however, such high-power devices typically oscillate in multiple modes, have limited beam quality often with significant sidelobes, and have limited tunability.[4,5,6,7,8] THz QC-lasers based on metal-metal waveguides exhibit improved temperature performance over SP waveguides, but suffer from even worse beam patterns and low outcoupling efficiency due to impedance mismatch and strong diffraction from their sub-wavelength radiating facets.[9] Metal-metal waveguide deficiencies have been greatly improved upon using a variety of design techniques such as distributed-feedback surface-emitting or end-fire cavities, photonic crystals, antenna-coupled cavities, etc., but so far none of these solutions have been scalable to watt-level output powers.[10,11,12,13] In recent years, an alternative architecture has been demonstrated by building THz QC-lasers in a vertical-external-cavity surface-emitting laser (VECSEL) configuration.[14] Such devices have been demonstrated to lase in single-mode with near-diffraction-limited Gaussian output beams, peak pulsed powers over 100 mW, and continuous wave powers over 5 mW at 77 K.[15,16,17]

The enabling component of the THz QC-VECSEL is an amplifying reflectarray metasurface. In its simplest form, it consists of an array of narrow metal-metal waveguide ridges, whose widths w are determined by the first-order resonance condition at the intended wavelength according to $w \approx \lambda_0/2n$ (n being the index of refraction within the semiconductor). These ridges act as low-quality-factor sub-cavities that couple to the master high-Q external-cavity mode. The structure of each sub-cavity is similar in form to an elongated patch antenna, in which the transverse electric-field $\vec{E}$ from each waveguide sidewall radiates according to equivalent magnetic current sources $\vec{M}_s = 2\hat{n} \times \vec{E}$, where $\hat{n}$ is the surface normal.[18,19] Although the E_y field for the TM_{01} mode is odd, $\hat{n}$ is also odd so that the sidewall magnetic currents $\vec{M}_s$ are in-phase for efficient surface normal radiation. In this letter, we introduce a metasurface design in which the metal-metal ridges are resonant in the TM_{03} lateral mode. The transverse field E_y has the same symmetry and therefore couples to surface incident radiation in the same manner as the TM_{01} ridges (see Fig. 1(a) and (b)). However, because the TM_{03} ridges are approximately three times as wide as the TM_{01} ridges for a given frequency, we increase the amount of gain material (and injection current) per unit area. This increased "fill factor" allows us to greatly increase the VECSEL output power without having to increase the overall dimensions of the

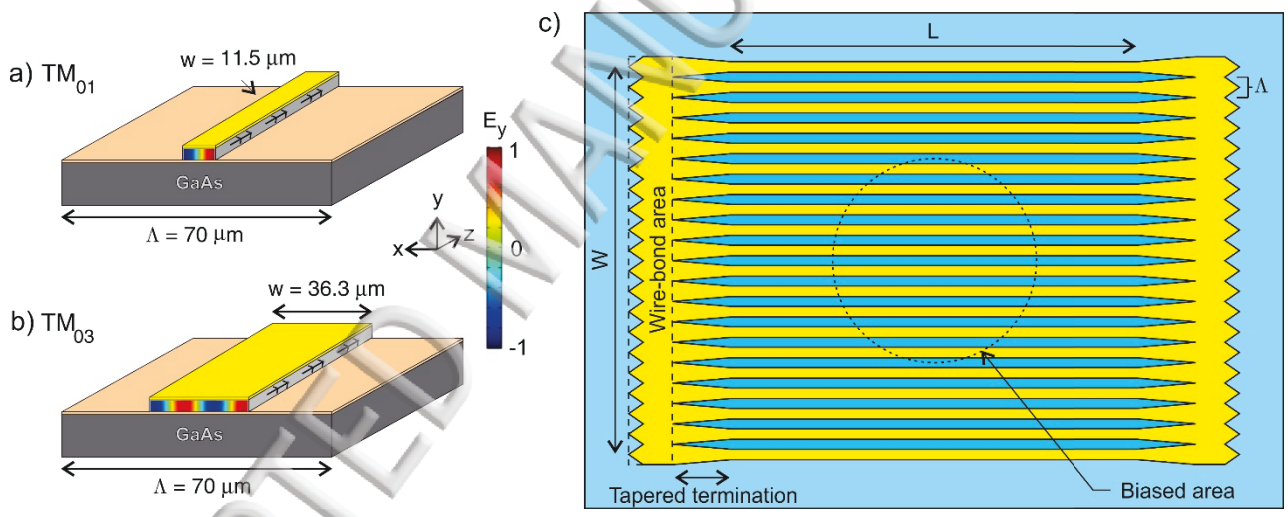

FIG. 1. Cross-sectional schematic of metasurface unit cell that illustrates the difference between (a) TM_{01} and (b) TM_{03} metasurface designs. (c) Areal view of TM_{03} metasurface. *W*=*L*=3 mm for fabricated devices and bias area diameter = 1.5 mm. The tapered terminations are 300 μm long, and each wirebond area is another 300 μm in length, making the total length of the metasurface 4.2 mm.

metasurface, and allows for more efficient use of the epitaxially grown wafer.

The TM_{03} metasurface was designed for operation at 3.4 THz using a finite-element electromagnetic solver. A single period of the metasurface structure was modeled in COMSOL Multiphysics with periodic boundary conditions, including losses within the metal and active region (see Ref. 15). The effect of a generic intersubband gain (equivalent to a frequency independent gain coefficient of 40 cm^{-1}) was included via an anisotropic permittivity (see Ref. 14). In Fig. 2, the simulated reflectance of a TM_{01} metasurface with a period Λ=70 μm and ridge width w = 11.5 μm (fill factor = 0.16) is compared to a TM_{03} metasurface

with a period Λ=70 μm and ridge width w = 36.3 μm (fill factor = 0.52). The two curves are quite comparable, and in fact, the TM_{03} metasurface gives slightly higher reflectance. In principle, a similar increase in fill factor could be accomplished with a TM_{01} design by simply reducing the period Λ. However, simulation results in Fig. 2 (dotted line) show that simply reducing the period of the TM_{01} structure (Λ = 24 μm, w = 12.5 μm, fill factor = 0.52) leads to much stronger coupling between neighboring ridges, which results in a metasurface with a much weaker peak reflectance. This broader resonant response

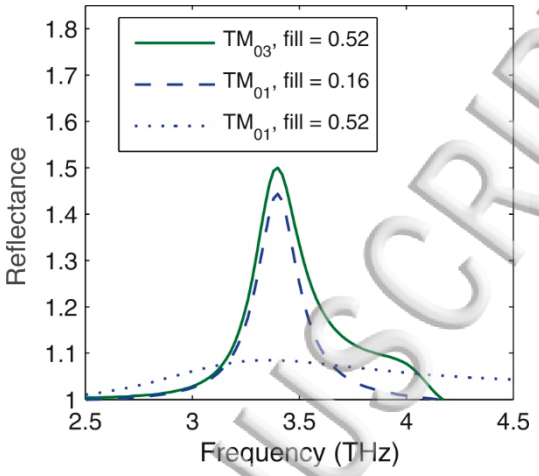

FIG. 2. Simulated reflectances for several metasurfaces when 40 cm^{-1} of intersubband gain is applied. Comparison is made between 70 μm period TM_{03} and TM_{01} surfaces, as well as a high fill factor TM_{01} surface with a 24 μm period.

corresponds to reduced field enhancement within the ridges. While this is not inherently bad, it makes the VECSEL more sensitive to any source of loss from the external cavity.[15]

TM_{03} metasurface devices were fabricated using the standard metal-metal (Cu-Cu) waveguide microfabrication techniques outlined in Refs. 14 and [20]. The metasurface selected for testing was a 3×3 mm^2 metasurface with tapered terminations leading to wire-bonding areas. By selectively depositing silicon dioxide between the GaAs/AlGaAs QC-laser material and the top Ti/Au metal contact, we electrically bias only a center circular area of 1.5 mm diameter in order to preferentially pump the fundamental transverse cavity mode. The 10 μm thick active region is grown by molecular beam epitaxy, and is based on the hybrid resonant-phonon/bound-to-continuum design concept [21]; it is the same design used by Li, *et al.* in Ref 4, and it is the same wafer as used in Refs. 15, 16 (wafer VB0739). The output couplers used were inductive and capacitive metal-meshes deposited on a 135 μm thick z-cut quartz substrate (see supplemental material Fig. S1). Both the metasurface and the output coupler were mounted inside the cryostat. This removes any windows from within the external cavity, as in Ref. 16. Also, in this work, we have added the ability to tune the length of the external cavity *in situ* by mounting the output coupler on a piezoelectric stepping stage (see supplemental material Fig. S2).

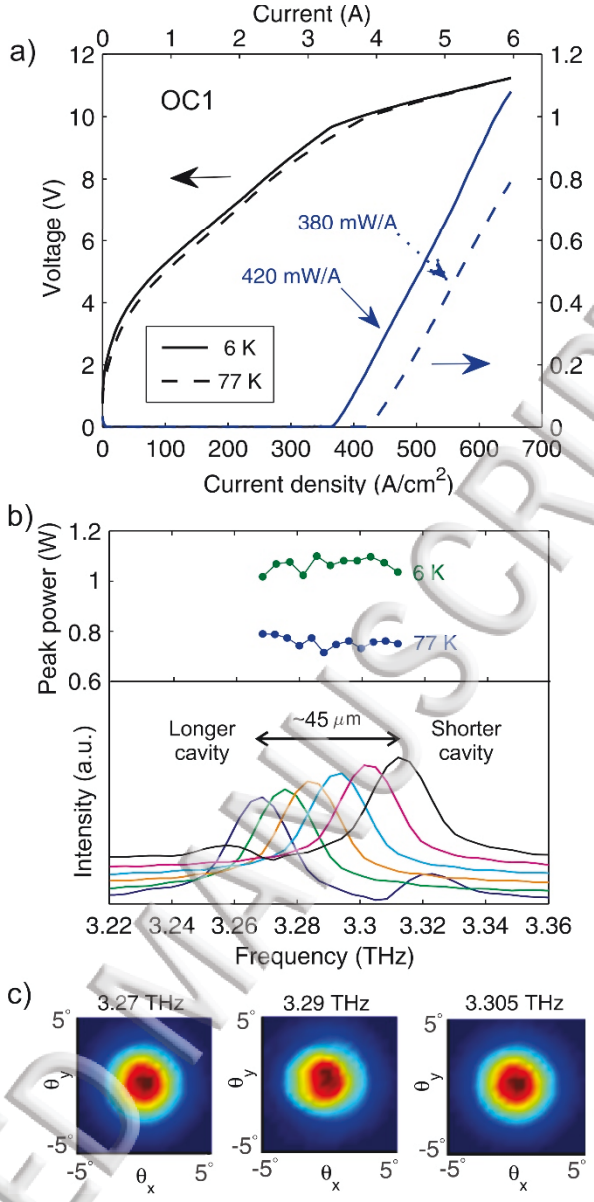

FIG. 3. (a) Pulsed-mode power and voltage vs. current characteristics from TM_{03} VECSEL using a highly reflective output coupler with a measured transmission of ~9%. (b) Normalized FTIR spectra collected as the VECSEL cavity length is tuned via a piezoelectric stepping stage, and corresponding output power as a function of frequency at 77 K and 6 K. (c) VECSEL far-field beam patterns.

Results using an inductive mesh output coupler with ~9% transmission (OC1) are plotted in Fig. 3. All measurements reported here were taken in pulsed mode (550 ns pulses at a 2 kHz repetition rate) as the large power dissipation prevents continuous-wave operation. Power vs. current (*P-I*) curves were measured with a pyroelectric detector (Gentec), and absolute power levels were measured using a calibrated thermopile. Peak power levels of 0.79 W and 1.1 W were measured at 77 K and 6 K respectively, and the output intensity with current is observed to be very linear with slope efficiencies (*dP/dI*) of 380 mW/A and 420 mW/A at 77 K and 6 K respectively. The cryostat was equipped with a parylene anti-reflection coated high-resistivity silicon window whose measured transmission is ~90% at 3.3 THz; the 10% window absorption has been accounted for in the

This manuscript was accepted by Appl. Phys. Lett. Click here to see the version of record.

reported power data. Spectra were measured using a Fourier-transform infrared (FTIR) spectrometer with 0.5 cm^{-1} resolution. By stepping the piezoelectric stage, continuous tuning of the laser frequency is observed from ~3.27-3.32 THz. This 50 GHz tuning range is limited by the free spectral range (FSR) of the external cavity; as the lasing mode is tuned away from the lowest threshold point, the adjacent longitudinal mode is tuned closer to the lowest threshold point and eventually a mode hop occurs. The change in cavity length as the VECSEL is tuned cannot be stated exactly as the piezoelectric stage is operated with an open-loop controller that does not have a position readout, but we can estimate its change since we know the cavity length must change by half of a wavelength to hop back to the starting frequency. The cavity FSR can be used to estimate the cavity length (~3 mm long in this case), but the FTIR does not allow the FSR to be determined with sufficient resolution to state an exact cavity length. The VECSEL characteristics (threshold, slope efficiency, output power, etc.) are influenced not only by the gain spectrum of the QC-material, but also by the spectral response of the metasurface and the reflectance of the output coupler. The reflectivity of the output coupler is relatively flat through the tuning range (see supplementary material Fig. S1), as is the measured output power (Fig 3(b)) and threshold current (see supplementary material Fig. S3), which suggests that the QC-gain material and the metasurface reflectance are also relatively constant through this range. A circular, high-quality beam with a full-width half-maximum divergence angle of ~4° is consistently observed as the VECSEL is tuned (see supplementary material Fig. S4 for Gaussian curve fitting to 1-D beam cuts). Two-axis beam measurements were performed using a 2-mm diameter pyroelectric detector scanned in a spherical pattern at a constant distance of 15 cm from the VECSEL (0.8° resolution).

Next, in Fig. 4 we present the VECSEL's performance using the same TM_{03} metasurface, but using a lower reflectance capacitive mesh output coupler, measured to have ~18% transmittance (OC2, see supplementary material Fig. S1). Threshold

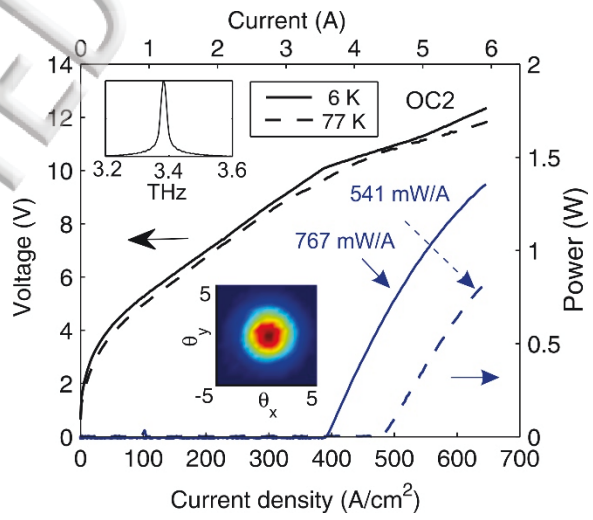

FIG. 4. *P-I-V* data from TM_{03} VECSEL using a low reflective output coupler with a measured transmission of ~18%. Note, the on-chip voltage probe failed during experiment, so voltage data was measured outside of cryostat (i.e. a two-terminal measurement) and scaled with a series resistance (see supplemental material Fig. S5).

currents, slope efficiencies, and maximum powers all increase at both 77 K and 6 K compared to when OC1 was used, which indicates that the laser is closer to the optimum outcoupling condition. A maximum peak power of ~1.35 W and peak slope efficiency of 767 mW/A is observed in a single mode with a narrow, Gaussian shaped beam and peak wall-plug efficiency of ~2% at 6 K (see Fig. 5). The lasing frequency when using OC2 was ~3.38 THz, slightly higher than OC1, which lased closer to 3.3 THz. This can be explained by observing that OC2 is more reflective at higher frequencies, which results in lower threshold currents at higher frequencies (see supplemental material Fig. S1). The VECSEL was again tuned through the cavity FSR of ~80 GHz, from 3.31-3.39 THz (cavity length ~1.9 mm), however, there is a strong atmospheric absorption line at ~3.335 THz that makes it difficult to accurately characterize the power and slope efficiency as a function of tuning (see supplementary material Fig. S6). It is notable that the *P-I* characteristic exhibits sub-linear behavior at higher injection currents (particularly at 6 K). This is not due to a heating effect, as short pulses are used, and no such sub-linear behavior is observed when using the same metasurface with OC1. We speculate that this sub-linear behavior may be due to the onset of additional lasing in propagating (i.e. guided) waveguide modes that do not radiate, but still compete with the TM_{03} VECSEL mode for gain. Indeed, the metasurface is observed to "self-lase" even in the absence of an output coupler, albeit at threshold currents higher than required to lase in the VECSEL mode (see supplementary material Fig. S7). However, the simultaneous lasing of guided modes along with the VECSEL mode cannot be readily verified given the limited resolution and dynamic range of our FTIR spectrometer since the guided modes don't radiate significantly, and any scattered power would be indiscernible from the high power of the VECSEL mode. This problem could be remedied in the future by making the metasurface even larger compared to the bias area (i.e. a 5×5 mm^2 metasurface with a 1.5 mm bias diameter rather than a 3×3 mm metasurface with a 1.5 mm bias diameter), so that the additional unbiased section would add more round-trip loss to the propagating modes. Alternatively, more loss could be added to the terminations by leaving a heavily doped GaAs contact layer exposed at the edges of the metal.[22]

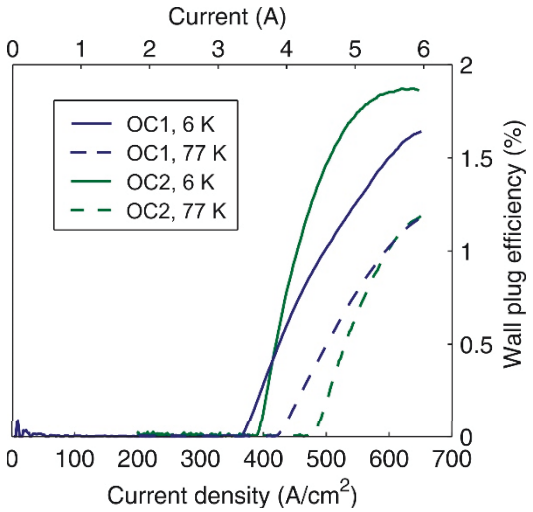

FIG. 5. Wall plug efficiency as a function of electrical pump power for the TM_{03} metasurface. Results for both OC1 and OC2 at 77 K and 6 K are presented.

In conclusion, we have demonstrated use of the third-order lateral resonance of metal-metal ridge waveguides to increase the peak output power of a THz QC-VECSEL to above 1 W in pulsed mode. Further increase of the THz QC-VECSEL power should be possible by making the metasurface even larger, or even moving to a TM_{05} resonant metasurface, should there be a need for such multi-watt level peak powers. However, our results suggest that increased efforts should be made in the future to suppress parasitic lasing of confined modes to prevent gain-competition and roll-over of the power-current characteristics. Additionally, by using piezoelectric intracryostat control of the cavity length, we have shown the potential of the VECSEL cavity to provide modest single-mode tunability of 1-2% without degrading the laser output power and while maintaining excellent beam quality.

Supplementary Material

See supplementary material for data on output couplers, illustrations of the VECSEL cavity construction, measurements of voltage-current characteristics, and additional data collected from the metasurface.

Acknowledgements

Microfabrication was performed at the UCLA Nanoelectronics Research Facility, and wire bonding was performed at the UCLA Center for High Frequency Electronics. This work was performed, in part, at the Center for Integrated Nanotechnologies, an Office of Science User Facility operated for the U.S. Department of Energy (DOE) Office of Science. Sandia National Laboratories is a multimission laboratory managed and operated by National Technology and Engineering Solution of Sandia, LLC., a wholly owned subsidiary of Honeywell International, Inc., for the U.S. Department of Energy's National Nuclear Security Administration under contract DE-NA-0003525. Partial funding was provided by the National Science Foundation (1407711, 1711892) and National Aeronautics and Space Administration (NNX16AC73G).

REFERENCES

1 M. S. Vitiello, G. Scalari, B. Williams, and P. De Natale, Opt Express **23** (4), 5167 (2015).
2 R. Kohler, A. Tredicucci, F. Beltram, H. E. Beere, E. H. Linfield, A. G. Davies, D. A. Ritchie, R. C. Iotti, and F. Rossi, Nature **417** (6885), 156 (2002).
3 B. S. Williams, S. Kumar, H. Callebaut, Q. Hu, and J. L. Reno, Appl Phys Lett **83** (11), 2124 (2003).
4 L. H. Li, L. Chen, J. X. Zhu, J. Freeman, P. Dean, A. Valavanis, A. G. Davies, and E. H. Linfield, Electron Lett **50** (4), 309 (2014).
5 L. H. Li, L. Chen, J. R. Freeman, M. Salih, P. Dean, A. G. Davies, and E. H. Linfield, Electron Lett **53** (12), 799 (2017).
6 H. Richter, N. Rothbart, and H. W. Hubers, J Infrared Millim Te **35** (8), 686 (2014).
7 A. W. M. Lee, B. S. Williams, S. Kumar, Q. Hu, and J. L. Reno, Opt Lett **35** (7), 910 (2010).

8 S. Chakraborty, O. Marshall, C. W. Hsin, M. Khairuzzaman, H. Beere, and D. Ritchie, Opt Express **20** (26), B306 (2012).

9 A. J. L. Adam, I. Kasalynas, J. N. Hovenier, T. O. Klaassen, J. R. Gao, E. E. Orlova, B. S. Williams, S. Kumar, Q. Hu, and J. L. Reno, Appl Phys Lett **88** (15) (2006).

10 M. I. Amanti, M. Fischer, G. Scalari, M. Beck, and J. Faist, Nat Photonics **3** (10), 586 (2009).

11 H. Zhang, L. A. Dunbar, G. Scalari, R. Houdre, and J. Faist, Opt Express **15** (25), 16818 (2007).

12 Y. Chassagneux, R. Colombelli, W. Maineult, S. Barbieri, S. P. Khanna, E. H. Linfield, and A. G. Davies, Appl Phys Lett **96** (3) (2010); G. Y. Xu, R. Colombelli, S. P. Khanna, A. Belarouci, X. Letartre, L. H. Li, E. H. Linfield, A. G. Davies, H. E. Beere, and D. A. Ritchie, Nat Commun **3** (2012).

13 L. Bosco, C. Bonzon, K. Ohtani, M. Justen, M. Beck, and J. Faist, Appl Phys Lett **109** (20) (2016).

14 L. Y. Xu, C. A. Curwen, P. W. C. Hon, Q. S. Chen, T. Itoh, and B. S. Williams, Appl Phys Lett **107** (22) (2015).

15 L. Y. Xu, C. A. Curwen, D. G. Chen, J. L. Reno, T. Itoh, and B. S. Williams, Ieee J Sel Top Quant **23** (6) (2017).

16 L. Y. Xu, C. A. Curwen, J. L. Reno, and B. S. Williams, Appl Phys Lett **111** (10) (2017).

17 L. Y. Xu, D. G. Chen, T. Itoh, J. L. Reno, and B. S. Williams, Opt Express **24** (21), 24117 (2016).

18 P. W. C. Hon, A. A. Tavallaee, Q. S. Chen, B. S. Williams, and T. Itoh, Ieee T Thz Sci Techn **2** (3), 323 (2012).

19 Constantine A. Balanis, *Advanced engineering electromagnetics*. (Wiley, New York, 1989), pp.xx.

20 B. S. Williams, S. Kumar, Q. Hu, and J. L. Reno, Opt Express **13** (9), 3331 (2005).

21 M. I. Amanti, G. Scalari, R. Terazzi, M. Fischer, M. Beck, J. Faist, A. Rudra, P. Gallo, and E. Kapon, New J Phys **11** (2009).

22 Y. Chassagneux, R. Colombelli, W. Maineult, S. Barbieri, H. E. Beere, D. A. Ritchie, S. P. Khanna, E. H. Linfield, and A. G. Davies, Nature **457** (7226), 174 (2009).

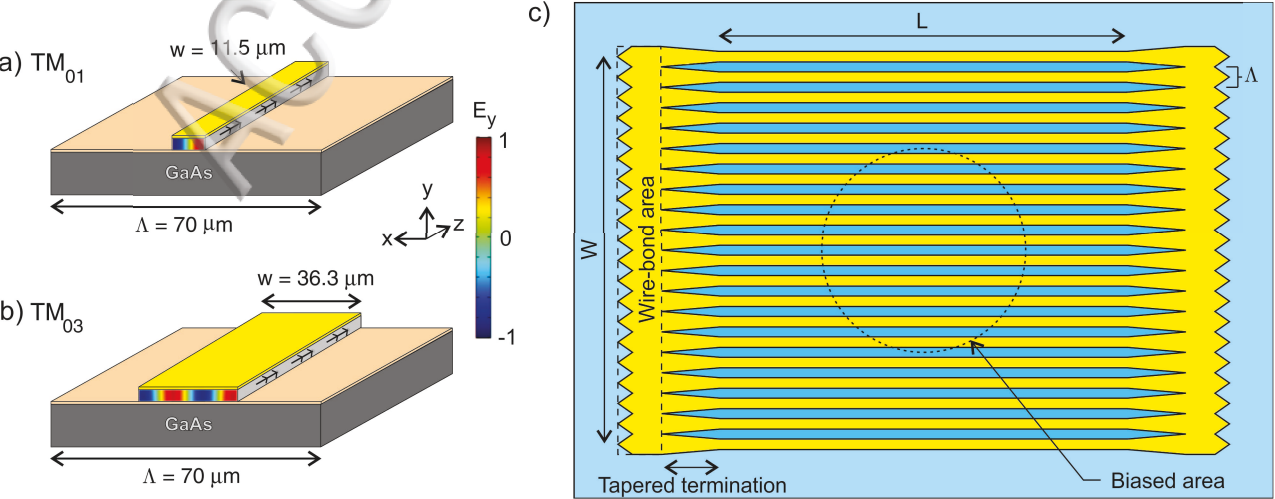
a) TM01
w = 11.5 μm
GaAs
Λ = 70 μm
Ey
1
0
-1
y
x
z
b) TM03
w = 36.3 μm
GaAs
Λ = 70 μm
c)
L
Λ
W
Wire-bond area
Tapered termination
Biased area

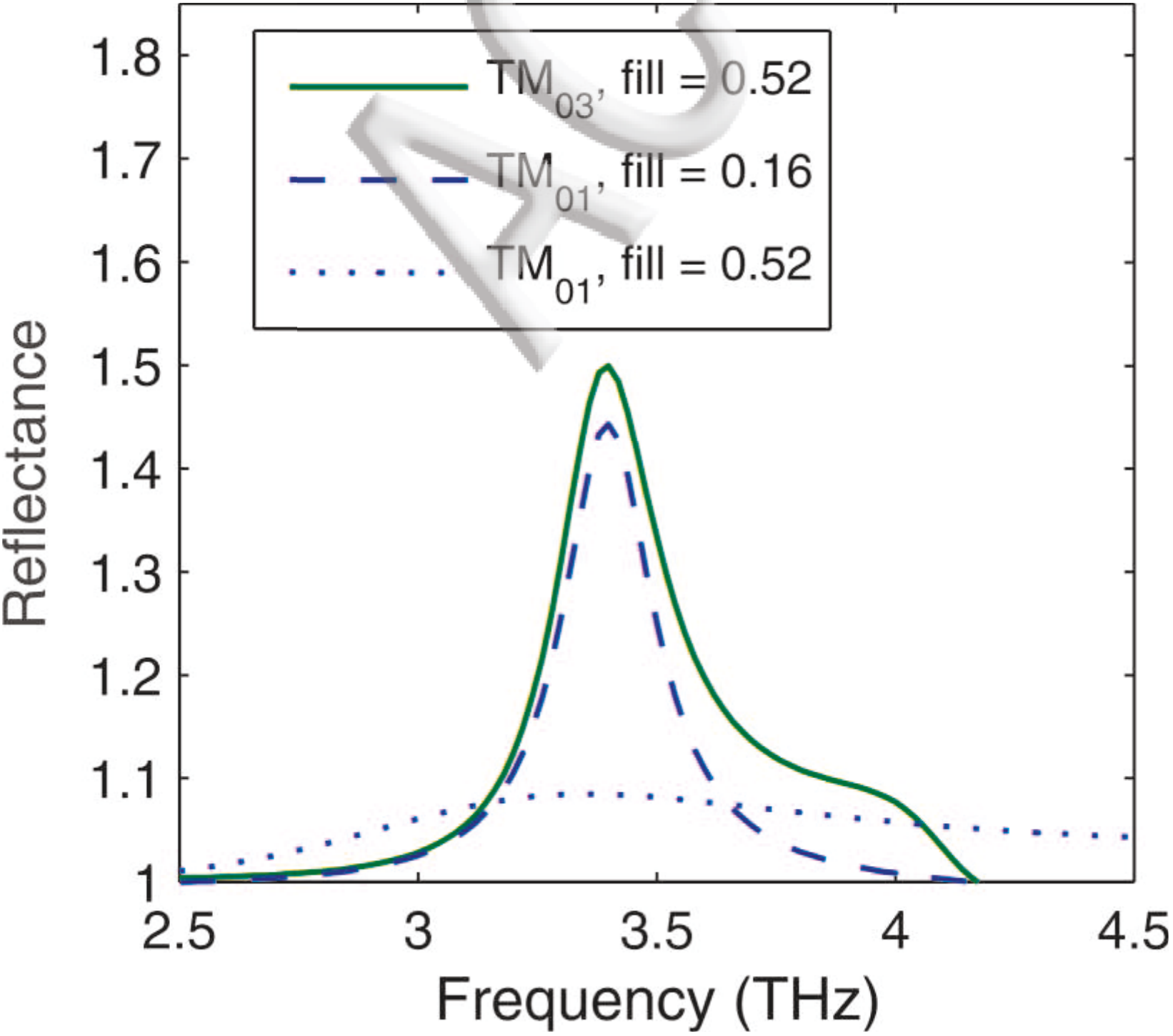
TM03, fill = 0.52
TM01, fill = 0.16
TM01, fill = 0.52
Reflectance
Frequency (THz)
1.8
1.7
1.6
1.5
1.4
1.3
1.2
1.1
1
2.5
3
3.5
4
4.5

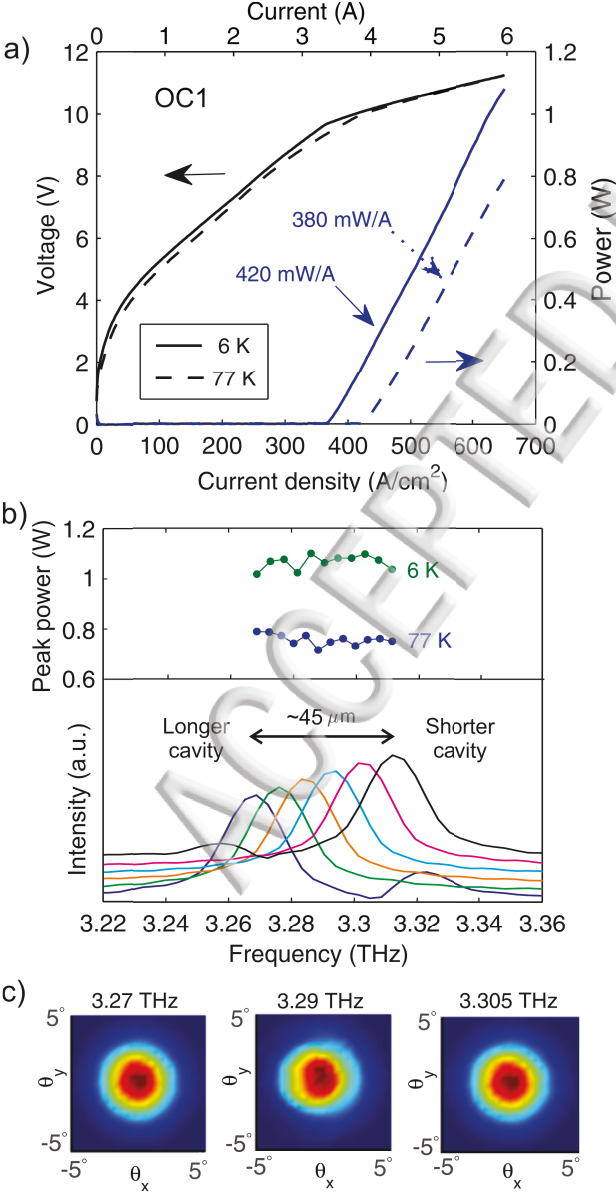
a)
Current (A)
OC1
Voltage (V)
Power (W)
380 mW/A
420 mW/A
6 K
77 K
Current density (A/cm^2)
b)
Peak power (W)
6 K
77 K
Longer cavity
~45 μm
Shorter cavity
Intensity (a.u.)
Frequency (THz)
c)
3.27 THz
3.29 THz
3.305 THz
θ_y
θ_x
5°
-5°

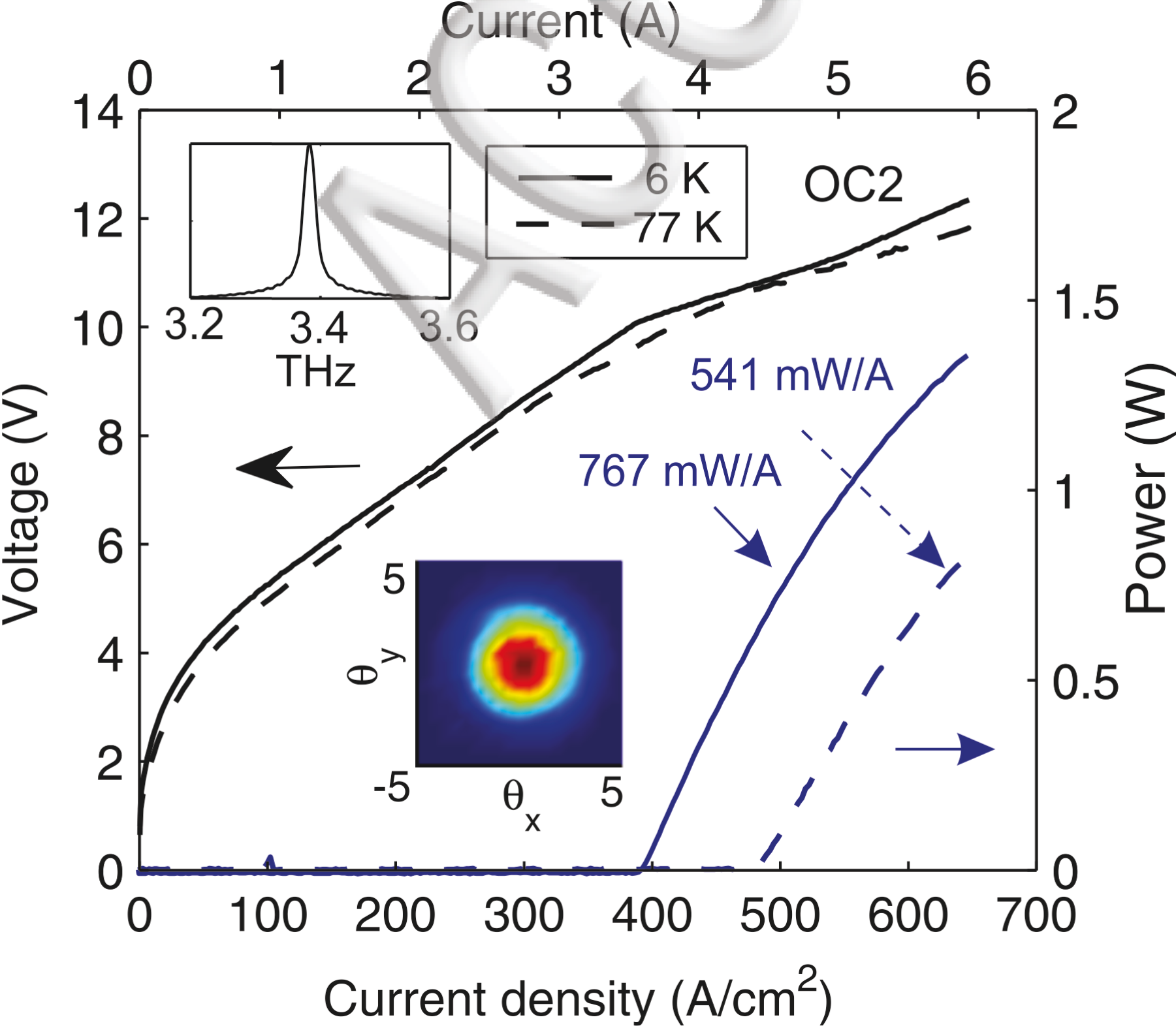
Current (A)
0
1
2
3
4
5
6
14
12
10
8
6
4
2
0
2
1.5
1
0.5
0
Voltage (V)
Power (W)
6 K
77 K
OC2
3.2
3.4
3.6
THz
541 mW/A
767 mW/A
5
-5
θy
θx
5
0
100
200
300
400
500
600
700
Current density (A/cm2)

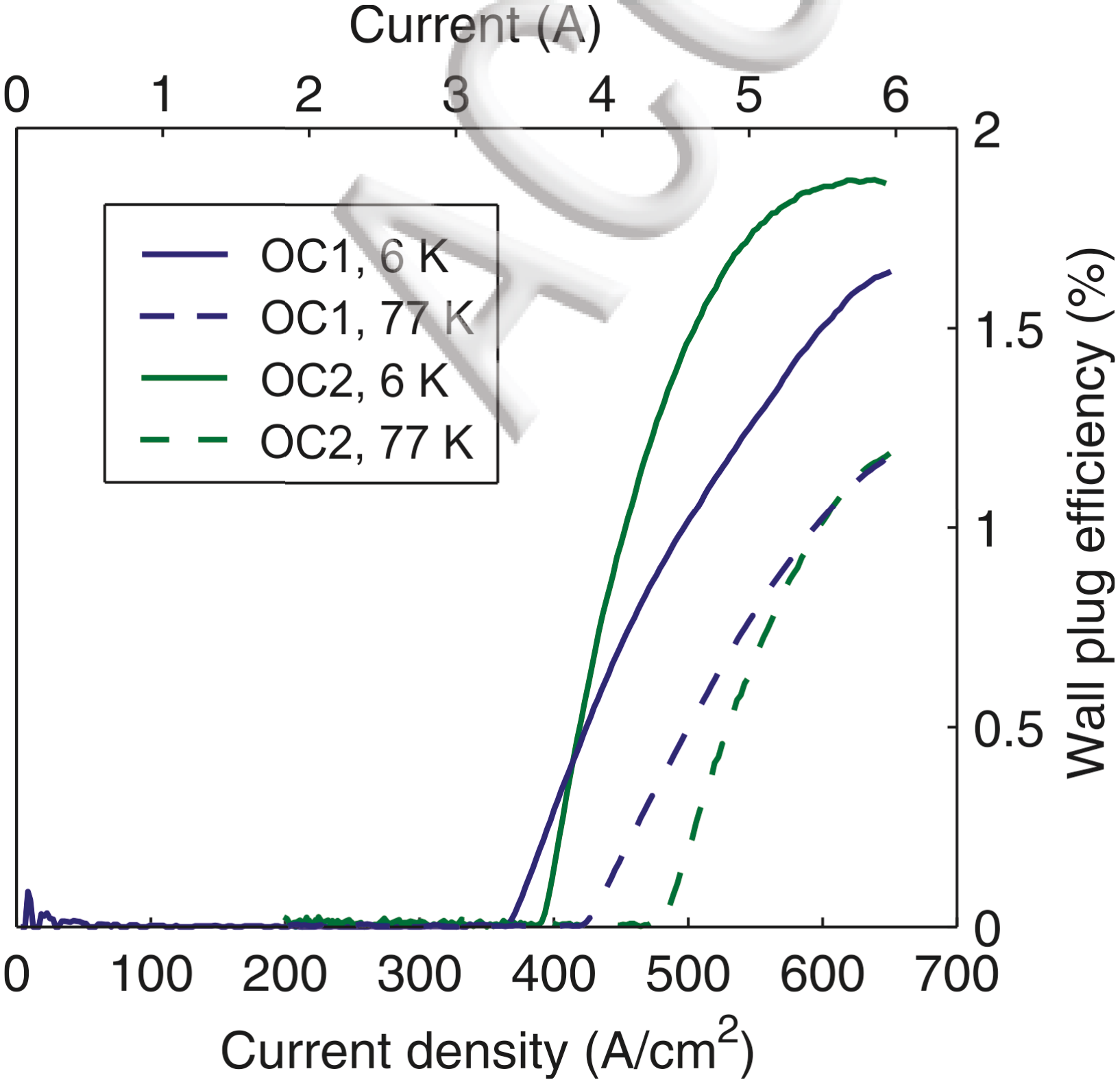
Current (A)
0
1
2
3
4
5
6
OC1, 6 K
OC1, 77 K
OC2, 6 K
OC2, 77 K
2
1.5
1
0.5
0
Wall plug efficiency (%)
0
100
200
300
400
500
600
700
Current density (A/cm2)